Three-dimensional process and device modeling

S.Selberherr and E. Langer
Institute for Microelectronics, Technical University, Gusshausstrasse 27-29, A-1040 Vienna, Austria

This contribution is intended to review the international state-of-the-art in three-dimensional process and device modeling. As one particular example, results for ion implantation into a three-dimensional trench are presented. Redistribution of dopants, interstitials and vacancies with fully coupled models is discussed. The recent refinements to carrier transport models in semiconductor devices are presented. As a particular example for three-dimensional device simulation the influence of the shape of the field-oxide in the width direction is discussed. Some remarks on the computational requirements are made.

1. Introduction

In the development of miniaturized devices for integrated circuits and particularly their technology, the demand for models capable of predicting the various processing steps of device fabrication and the electrical behavior of devices is growing dramatically owing to the tight coupling of electrical device effects with the doping profile.

It is not possible to give an extensive overview here of all the international activities on three-dimensional process and device modeling. This paper has therefore been restricted to the description of some interesting and recently performed investigations.

2. Process modeling

Device fabrication processes can be principally categorized into two groups: lithographic processes which serve patterning purposes and doping processes which determine, for a given structure, the electrical properties of the intended semiconductor device. The first group consists of deposition and etching with spatial selectivity in order to enable structuring. It may be viewed as a fixed process which provides flexibility in layout. The second group is composed of ion implantation, diffusion, thermal oxidation and epitaxy.

This section deals with a simulation of ion implantation into a three-dimensional trench [1] and with a new model of phosphorus diffusion in silicon [2] including the redistribution of dopants, interstitials and vacancies.

2.1 Ion implantation into a three-dimensional trench

Ion implantation is doubtless a central point in the fabrication of semiconductor devices. Therefore, as one particular example of three-dimensional process modeling, results for ion implantation into a three-dimensional trench are presented in this section. In order to demonstrate the necessity of three-dimensional process simulation tools the two-dimensional solution is shown for comparison.

The calculations have been performed with a two- and three-dimensional program package for the simulation of ion implantation based on the "Monte Carlo" method, including some additional features to increase computational efficiency [1]. The first step in the development of that software tool was a two-dimensional model of ion implantation which accounted for position dependent lateral moments [3]. With this model the analytical des-

cription of ion implantation profiles has been essentially improved by specifying a modification of the Gaussian distribution function. The benefit of the use of distribution functions evidently lies in the low computer resources required. The enormous drawback is the restriction of the applicability to simple geometries only. To investigate ion implantation in connection with arbitrary geometries a rigorous simulation method has to be applied.

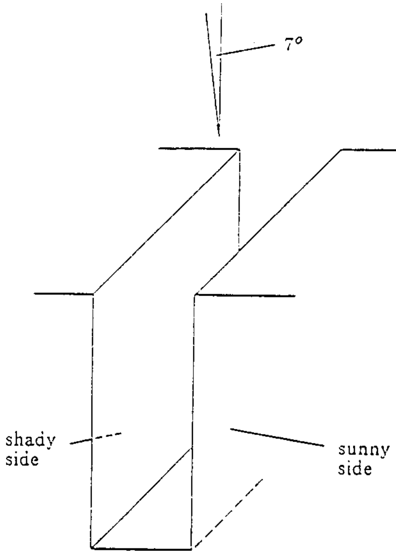

Fig. 1 Two-dimensional trench

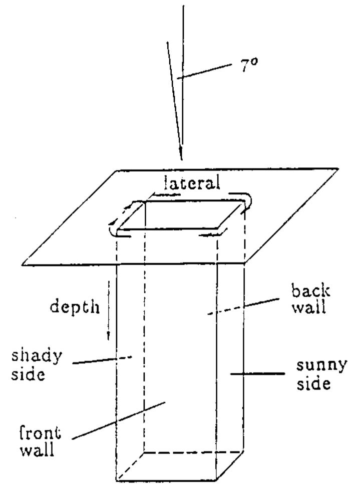

Fig. 2 Three-dimensional trench with square cross-section

Figures 1 and 2 show the geometry of the investigated trench for the two- and three-dimensional case, respectively. The three-dimensional trench has a square cross-section. The substrate material is silicon in which boron ions are implanted with an energy of 25 keV. The angle of incidence of the ion ray is 7° with respect to the perpendicular of the wafer surface.

Figures 3 and 4 show the concentration of dopants in a quasi three-dimensional representation as a result of the two- and three-dimensional simulation, respectively. The result of the three-dimensional simulation (Fig. 4) is displayed for the symmetry plane between front wall and back wall (see Fig. 2). The surface of the wafer is located on the left side of the top of the drawings. The vertical axis denotes the logarithm of the boron concentration divided by the implantation dose. The left axis lies parallel to the shady side of the trench and represents the depth whereas the right axis is parallel to the bottom of the trench and represents the width. Regarding Fig. 3 one can see the considerable concentration on the shady side which is just about a factor of 5 smaller than the concentration on the sunny side. A comparison between Fig. 3 and Fig. 4 shows on the one hand that the concentrations on the sunny sides are rather the same, but on the other hand the concentrations on the shady side differ by about a factor of 2. Such an inaccuracy of the two-dimensional simulation is certainly not acceptable as small variations of a doping profile persistently influence the electrical behaviour of a semiconductor device.

2.2 Phosphorus diffusion in silicon

Under extrinsic concentrations the diffusion of phosphorus in silicon shows a considerable deviation from the Gaussian, the complementary error-function distributions or concentration distributions of other dopants. The phosphorus profile has a "kink and tail" dif-

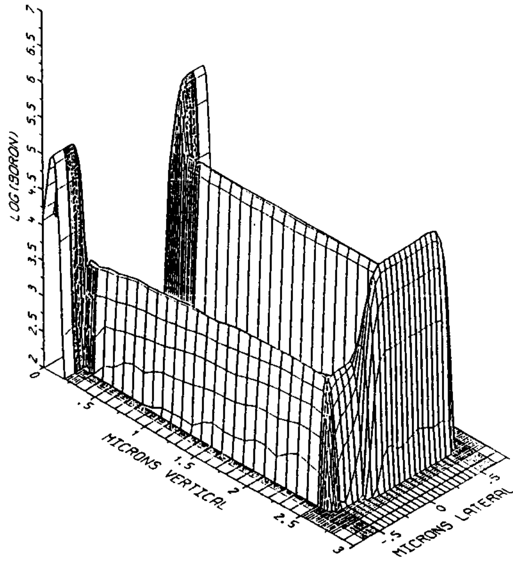

Fig. 3 Concentration of dopants in the two-dimensional trench

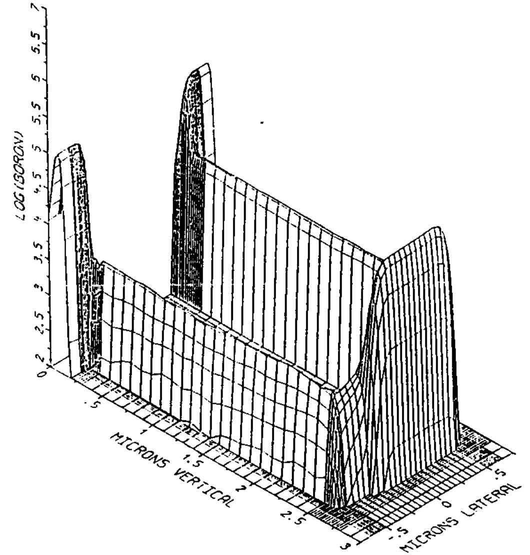

Fig. 4 Concentration of dopants in the symmetry plane of the three-dimensional trench

fusion behaviour. The diffusion coefficient in the intrinsic region under thermal annealing conditions depends on the surface concentration of phosphorus. This diffusion is faster than the diffusion in the lower concentration part of the extrinsic region. In the high concentration part of the extrinsic region the diffusion is proportional to the square of the electron concentration. From coupled diffusion with other dopants and stacking fault growth it is known that phosphorus produces a supersaturation on interstitials in the "tail" region depending on the surface concentration of the profile [4].

The model developed to describe the anomalous phosphorus diffusion in silicon [2] is based on the motion of impurity-point defect pairs. Though the following derivation is layed out for one spatial dimension the model evidently is applicable to two- and three-dimensional simulations. The impurity (A) can react with point defects (D) (interstitials and vacancies)

$$AD \rightleftharpoons A + D \tag{1}$$

The point defects and impurity-point defect pairs have different charge states and react with electrons or holes.

$$D^{i-1} \rightleftharpoons D^i + e^- \ , \ D^{i+1} \rightleftharpoons D^i + h^+ \tag{2}$$

$$AD^{i-1} \rightleftharpoons AD^i + e^- \ , \ AD^{i+1} \rightleftharpoons AD^i + h^+ \tag{3}$$

For all these combinations a diffusion equation describes the motion through the bulk including the electrical potential ψ which is normalised to the thermal potential. The substitutional dopants are assumed not to diffuse at all. Therefore the following expressions are obtained for the particle current densities

$$J^i_{AD} = -D^i_{AD} \left(\frac{\partial c^i_{AD}}{\partial x} - (i - d(A))\, c^i_{AD} \frac{\partial \psi}{\partial x} \right) \tag{4}$$

$$J^i_D = -D^i_D \left(\frac{\partial c^i_D}{\partial x} - i c^i_D \frac{\partial \psi}{\partial x} \right), \; J_A = 0 \tag{5}$$

in which d(A) denotes the charge state of the dopant ion. The number of these equations can be reduced under the assumption that the reaction with the electrons and holes happens very fast and the charge states are in thermal equilibrium. The different concentrations c^i_{AD} are summed to a total concentration c_{AD}. Similarly a total point defect concentration c_D is defined.

$$c^i_{AD} = k^i_{AD} c^0_{AD} \left(\frac{n}{n_i} \right)^i, \quad c^i_D = k^i_D c^0_D \left(\frac{n}{n_i} \right)^i \tag{6}$$

$$c_{AD} = \Sigma_i\, c^i_{AD}, \quad c_D = \Sigma_i\, c^i_D \tag{7}$$

The new current equations yield a mean diffusion coefficient and a mean electrical charge $\overline{Q}$ depending on the electron concentration.

$$J_{AD} = -\overline{D}_{AD} \left(\frac{\partial c_{AD}}{\partial x} + \overline{Q}_{AD} c_{AD} \frac{\partial \psi}{\partial x} \right)$$

$$J_D = -\overline{D}_D \left(\frac{\partial c_D}{\partial x} + \overline{Q}_D c_D \frac{\partial \psi}{\partial x} \right) \tag{8}$$

$$\overline{D}_{AD} = \frac{\Sigma_i D^i_{AD} k^i_{AD} (n/n_i)^i}{\Sigma_i k^i_{AD} (n/n_i)^i}$$

$$\overline{D}_D = \frac{\Sigma_i D^i_D k^i_D (n/n_i)^i}{\Sigma_i k^i_D (n/n_i)^i} \tag{9}$$

$$\overline{Q}_{AD} = \frac{\Sigma_i (d(A) - i) k^i_{AD} (n/n_i)^i}{\Sigma_i k^i_{AD} (n/n_i)^i}$$

$$\overline{Q}_D = \frac{\Sigma_i -i k^i_D (n/n_i)^i}{\Sigma_i k^i_D (n/n_i)^i} \tag{10}$$

The formation of AD-pairs and the decay into their components is expressed by a generation term G_{AD} which accounts for the tendency towards thermal equilibrium. The "Frenkel pair" mechanism is described by G_F ($I + V \rightleftharpoons 0$).

$$\frac{\partial c_{AD}}{\partial t} + \frac{\partial J_{AD}}{\partial x} = -G_{AD}$$

$$\frac{\partial c_A}{\partial t} = \Sigma_D \, G_{AD} \tag{11}$$

$$\frac{\partial c_D}{\partial t} + \frac{\partial J_D}{\partial x} = \Sigma_A \, G_{AD} + G_F$$

$$G_{AD} = k_{decay} \, c_{AD} \, \Sigma_i \, k^i_D \, (n/n_i)^i - k_{generation} \, c_A c_D \, \Sigma_i \, k^i_{AD} \, (n/n_i)^i \tag{12}$$

In this form the model needs three equations for each species plus two for the point defects. The boundary conditions for point defects are set to their thermal equilibrium values dependent on the electron concentration. C_D^{eq} is the thermal equilibrium value under intrinsic conditions for vacancies and interstitials.

$$c_D = c_D^{eq} \frac{\Sigma_i \, k^i_D \, (n/n_i)^i}{\Sigma_i \, k^i_D} \tag{13}$$

For the impurities and impurity-pairs the boundary conditions are either $J_{AD} = 0$ and $J_D = 0$ or a constant concentration under consideration of the thermal equilibrium condition for the reaction between impurities and point defects.

$$c_{AD} = F_{AD} c_A c_D \, , \; F_{AD} = \frac{k_{generation} \, c_A c_D \, \Sigma_i \, k^i_{AD} \, (n/n_i)^i}{k_{decay} \, c_{AD} \, \Sigma_i \, k^i_D \, (n/n_i)^i} \tag{14}$$

Figure 5 shows a comparison between calculation and measurement of a profile generated by a coupled phosphorous–boron diffusion experiment. The doping profile has been measured by SIMS (dashed lines). The calculation has been performed by implementing the diffusion model into the program package ZOMBIE [5], which is a one-dimensional general solver for systems of coupled parabolic, elliptic, and ordinary differential equations with non-constant coefficients. The good agreement between calculation and measurement can be explained by the fact that the diffusion model takes into account both the vacancies and interstitials.

3. Device modeling

Since silicon VLSI technology has evolved to a standard that hundreds of thousands of transistor devices are integrated in a single chip it has become crucial to understand even second-order effects of basic device operation. The application of numerical simulation packages for the development of prototype devices is therefore a basic requirement.

Device modeling based on the self-consistent solution of the well-known fundamental

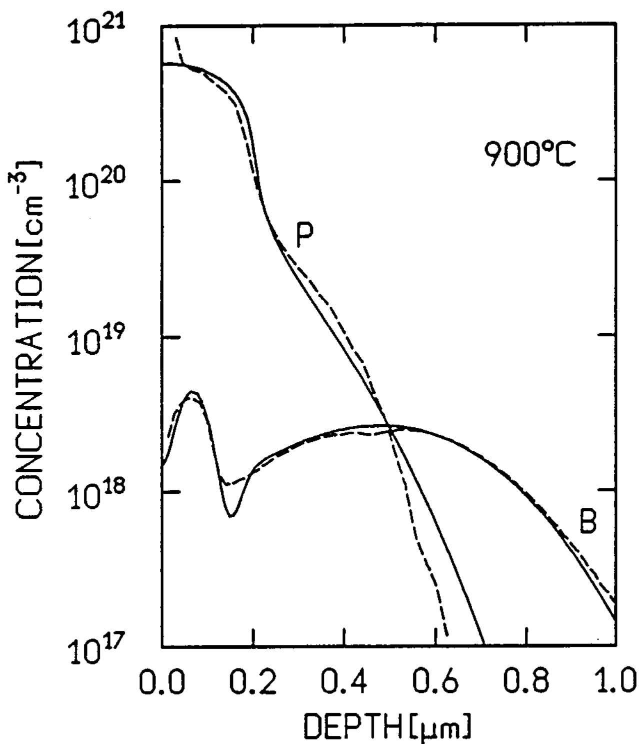

Fig. 5 Doping profile of a coupled diffusion experiment

semiconductor equations [6] dates back to the famous work of Gummel [7] in 1964. Since then numerical device modeling has been applied to nearly all important devices. Today there are ongoing arguments in the scientific community whether the semiconductor equations are adequate to describe transport in submicron devices. Particularly the current relations (15) and (16) which are the most complex equations out of the set of the basic semiconductor equations undergo strong criticism in view of, for instance, ballistic transport [8,9]. Their derivation from more fundamental physical principles is indeed not at all straightforward. They appear therefore with all sorts of slight variations in the specialized literature and a vast number of papers has been published where some of their subtleties are dealt with. The interested reader is referred, for example, to refs. 10–13. Anyway, recent investigations on ultrashort MOSFETs [14] do not give evidence that it is necessary to waive these well-established basic equations for silicon devices down to feature sizes in the order of 0.1 µm [15].

$$\vec{J}_n = q\,\mu_n\,n\left(\vec{E} + \frac{1}{n}\,\text{grad}\left(n\,\frac{k\,T_p}{q}\right)\right) \tag{15}$$

$$\vec{J}_p = q\,\mu_p\,p\left(\vec{E} + \frac{1}{p}\,\text{grad}\left(p\,\frac{k\,T_n}{q}\right)\right) \tag{16}$$

In this paper recent refinements to models of physical parameters concerning the current relations, namely the carrier mobilities and carrier temperatures are discussed. Further-

more, the influence of the shape of the field-oxide in width direction is presented as a particular example for three-dimensional device simulation.

3.1 Modeling carrier mobilities

The models of carrier mobilities μ_n and μ_p have to take into account a great variety of scattering mechanisms the most basic one of which is lattice scattering. The lattice mobility in pure silicon can be fitted with simple power laws

$$\mu_n^L = 1430 \frac{cm^2}{V\,s} \left(\frac{T}{300\,K}\right)^{-2}$$

$$\mu_p^L = 460 \frac{cm^2}{V\,s} \left(\frac{T}{300\,K}\right)^{-2.18} \tag{17}$$

The expressions (17) fit experimental data of refs. 16–18 well.

The next effect to be considered is ionised impurity scattering. The best established procedure for this task is to take the functional form (18) of the fit provided by Caughey and Thomas [19] and to use temperature-dependent coefficients.

$$\mu_{n,p}^{LI} = \mu_{n,p}^{min} + \frac{\mu_{n,p}^{L} - \mu_{n,p}^{min}}{1 + (CI/C_{n,p}^{ref})^{\alpha_{n,p}}} \tag{18}$$

$$\mu_n^{min} = \begin{cases} 80 \dfrac{cm^2}{V\,s} \left(\dfrac{T}{300\,K}\right)^{-0.45} & T \geqslant 200\,K \\[2ex] 80 \dfrac{cm^2}{V\,s} \left(\dfrac{200\,K}{300\,K}\right)^{-0.45} \left(\dfrac{T}{200\,K}\right)^{-0.15} & T < 200\,K \end{cases} \tag{19}$$

$$\mu_p^{min} = \begin{cases} 45 \dfrac{cm^2}{V\,s} \left(\dfrac{T}{300\,K}\right)^{-0.45} & T \geqslant 200\,K \\[2ex] 45 \dfrac{cm^2}{V\,s} \left(\dfrac{200\,K}{300\,K}\right)^{-0.45} \left(\dfrac{T}{200\,K}\right)^{-0.15} & T < 200\,K \end{cases} \tag{20}$$

$$C_n^{ref} = 1.12 \times 10^{17}\ \mathrm{cm^{-3}} \left(\frac{T}{300\ \mathrm{K}}\right)^{3.2}$$

$$C_p^{ref} = 2.23 \times 10^{17}\ \mathrm{cm^{-3}} \left(\frac{T}{300\ \mathrm{K}}\right)^{3.2} \qquad (21)$$

$$\alpha_{n,p} = 0.72 \left(\frac{T}{300\ \mathrm{K}}\right)^{0.065} \qquad (22)$$

The fits for eqns. (19)–(22) are from ref. 20; similar data have been provided in refs. 21 and 22.

In view of partial ionisation one should consider neutral impurity scattering [6]. However, in view of the uncertainty of the quantitative values for ionised impurity scattering introducing another scattering mechanism with additional fitting parameters does not seem worthwhile. Furthermore, partial ionisation appears to be a second-order effect even at liquid nitrogen temperature. It therefore seems justified to include partial ionisation only in the space charge model and not in the carrier mobilities.

Surface scattering is modeled with an expression suggested by Seavey [23].

$$\mu_{n,p}^{LIS} = \frac{\mu_{n,p}^{ref} + (\mu_{n,p}^{LI} - \mu_{n,p}^{ref})(1 - F(y))}{1 + F(y)\,(S_{n,p}/S_{n,p}^{ref})^{\alpha_{n,p}}} \qquad (23)$$

$$\mu_n^{ref} = 638\ \frac{\mathrm{cm^2}}{\mathrm{V\,s}} \left(\frac{T}{300\ \mathrm{K}}\right)^{-1.19}$$

$$\mu_p^{ref} = 160\ \frac{\mathrm{cm^2}}{\mathrm{V\,s}} \left(\frac{T}{300\ \mathrm{K}}\right)^{-1.09} \qquad (24)$$

with:

$$F(y) = \frac{2 \exp(-(y/y^{ref})^2)}{1 + \exp(-2(y/y^{ref})^2)} \qquad (25)$$

$$S_n = \max\left(0, \frac{\partial \psi}{\partial y}\right), \qquad S_p = \max\left(0, -\frac{\partial \psi}{\partial y}\right) \qquad (26)$$

S_n^{ref} is assumed to be 7×10^5 V cm^{-1}; S_p^{ref} is 2.7×10^5 V cm^{-1} and y^{ref} is 10 nm.

The formulae for surface scattering are definitely not the ultimate expressions. They just fit experimental observations reasonably. Other approaches with the same claim can be found in, e.g. refs. 9,25,26. A u-shaped mobility behaviour as found in refs. 27 and 28 has not been synthesised because we believe in a different origin than surface scattering for this experimental observation. It should be noted, however, that soft turn-on at liquid nitrogen

temperature has been successfully simulated with a u-shaped mobility expression [29].

Velocity saturation is modeled with eqns. (27). These are again fits to experimental data with, however, a theoretical background considering their functional form [16,30,31]

$$\mu_n^{LISE} = \frac{2\,\mu_n^{LIS}}{1 + \left[1 + (2\,\mu_n^{LIS} E_n/v_n^{sat})^2\right]^{1/2}}$$
$$\mu_p^{LISE} = \frac{\mu_p^{LIS}}{1 + \mu_p^{LIS} E_p/v_p^{sat}} \qquad (27)$$

E_n and E_p are the effective driving forces given by eqn. (28). Their derivation can be found in ref. 32.

$$E_n = \left| \text{grad}\,\psi - \frac{1}{n}\,\text{grad}\,(Ut_n\, n) \right|$$
$$E_p = \left| \text{grad}\,\psi + \frac{1}{p}\,\text{grad}\,(Ut_p\, p) \right| \qquad (28)$$

The saturation velocities are given by

$$v_n^{sat} = 1.45 \times 10^7\,\frac{\text{cm}}{\text{s}} \left[\tanh\,\frac{155\text{ K}}{T}\right]^{1/2}$$
$$v_p^{sat} = 9.05 \times 10^6\,\frac{\text{cm}}{\text{s}} \left[\tanh\,\frac{312\text{ K}}{T}\right]^{1/2} \qquad (29)$$

The functional form of these fits is after Ali-Omar and Reggiani [16]; the experimental data matched are from refs. 16,17,33,34. An eventual dependence on the crystallographic orientation which one would deduce from refs. 35–37, is not presently taken into account.

3.2 Modeling carrier temperatures

To describe carrier heating properly one has to account for local carrier temperatures $T_{n,p}$ in the current relations (15) and (16). This can be achieved by either solving energy conservation equations self consistently with the basic transport equations, or by using a model obtained by series expansions of the solution to the energy conservation equations [31]. We believe that the latter is sufficient for silicon devices. For the electronic voltages we have eqn. (30) as an approximation. Confirming theoretical investigations can be found in ref. 39.

$$Ut_{n,p} = \frac{kT_{n,p}}{q} = Ut_o + \frac{2}{3}\,\tau_{n,p}^{\varepsilon}\,(v_{n,p}^{sat})^2 \left(\frac{1}{\mu_{n,p}^{LISE}} - \frac{1}{\mu_{n,p}^{LIS}}\right) \qquad (30)$$

The energy relaxation times $\tau^{\varepsilon}_{n,p}$ are in the order of 0.5 ps and just weakly temperature dependent [39]. They should, however, be modeled as functions of the local doping concentration as motivated by the following reasoning. The product of carrier mobility and electronic voltage which symbolises a diffusion coefficient must be a decreasing function with increasing carrier voltage (see also ref. 39). Its maximum is attained at thermal equilibrium. Relation (31) must therefore hold.

$$\mu^{LISE}_{n,p}\, Ut_{n,p} \leqslant \mu^{LIS}_{n,p}\, Ut_{o} \qquad (31)$$

Note that models for carrier diffusion coefficients are not required in the basic current relations (15) and (16).

Substituting eqn. (30) into eqn. (31) and rearranging terms one obtains relation (32) for the energy relaxation times.

$$\tau^{\varepsilon}_{n,p} < \frac{3}{2}\, Ut_{o}\, \frac{\mu^{LIS}_{n,p}}{(v^{sat}_{n,p})^{2}} \qquad (32)$$

In the actual version of MINIMOS [40], the energy relaxation times are modeled on the basis of eqn. (32) with a “fudge factor” γ in the range [0,1] and a default value of 0.8.

$$\tau^{\varepsilon}_{n,p} = \gamma\, \frac{3}{2}\, Ut_{o}\, \frac{\mu^{LIS}_{n,p}}{(v^{sat}_{n,p})^{2}} \qquad (33)$$

For vanishing doping one obtains the maximum energy relaxation times which are at 300 K $\tau^{\varepsilon}_{n} = 4.44\times10^{-13}$ s, $\tau^{\varepsilon}_{p} = 2.24\times10^{-13}$ s and at liquid nitrogen temperature $\tau^{\varepsilon}_{n} = 8.82\times10^{-13}$ s, $\tau^{\varepsilon}_{p} = 8.68\times10^{-13}$ s.

3.3 Three-dimensional MOSFET simulation

This section presents three-dimensional effects of MOSFETs due to the non-planar nature of the field-oxide body. The investigations have been carried out by MINIMOS 5 [40] which is the latest extension of the program package used worldwide, now including all three spatial dimensions. Three-dimensional effects such as threshold shift for small channel devices, channel narrowing and the enhanced conductivity at the channel edge have been successfully modeled.

The geometry of the three-dimensional MOSFET investigated is given in Fig. 6: an n-channel with an 1 µm × 1 µm channel and gate oxide of 15 nm. The oxide body of the analysed structure can be seen in Fig. 7 (note that the oxide is between the upper and the lower plane). In order to demonstrate the effects at the channel edge two different bias points were selected. This first is near the threshold with $U_S = U_B = 0.0$ V, $U_D = 1.0$ V, $U_G = 0.5$ V (the threshold voltage for this device is $U_{th} \sim 0.75$ V). The potential distribution in channel length and width direction at the semiconductor/gate-oxide interface is shown in Fig. 8. (This plane penetrates into the field oxide near the contact boundary of source and drain). The corresponding minority carrier distribution is given in Fig. 9. A remarkable depletion region at the drain side causes the channel charge to be smaller (under certain bias conditions) than predicted by two-dimensional simulations. The second bias point is far above threshold $U_S = U_B = 0.0$ V, $U_D = 1.0$ V, $U_G = 3.0$ V. The corresponding potential distribution can be seen in Fig. 10. The location of the plane for which the distribution is

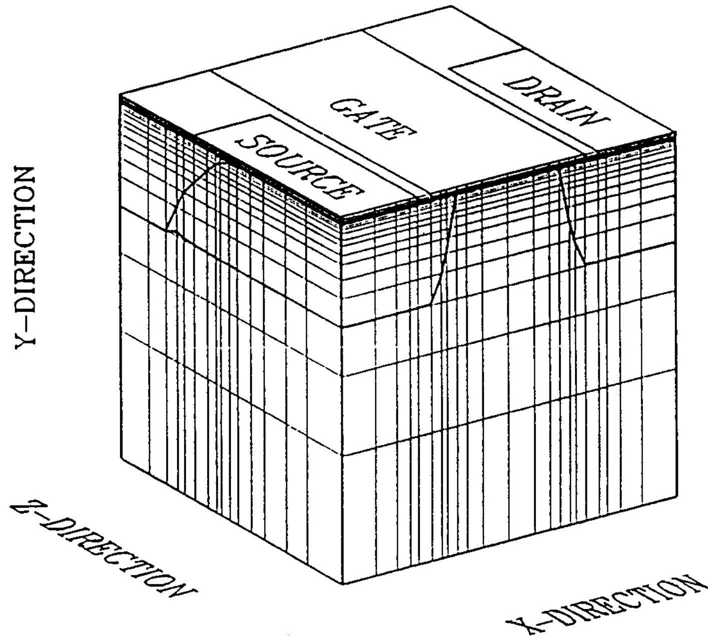

Fig. 6 Three-dimensional MOSFET structure

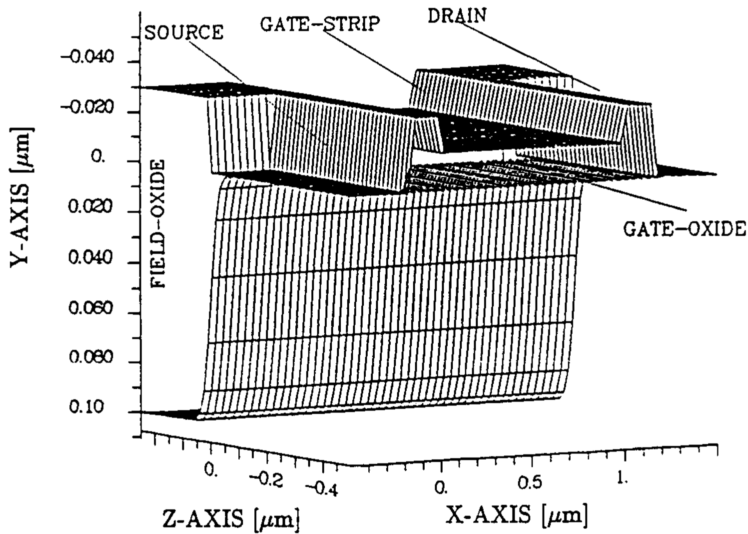

Fig. 7 Oxide body of the MOSFET structure

drawn is the same as the previous bias condition. The high increase of the potential distribution out of the channel is because the gate contact overlaps the field oxide. Also of interest is the minority carrier distribution (Fig. 11) which shows the enhanced conductivity at the semiconductor field-oxide interface. Note that only half of the channel width is shown in Figs. 8–11; −0.5 μm denotes the middle of the channel width and 0.0 μm the boundary of source and drain contacts. The consequence of the device characteristics of these

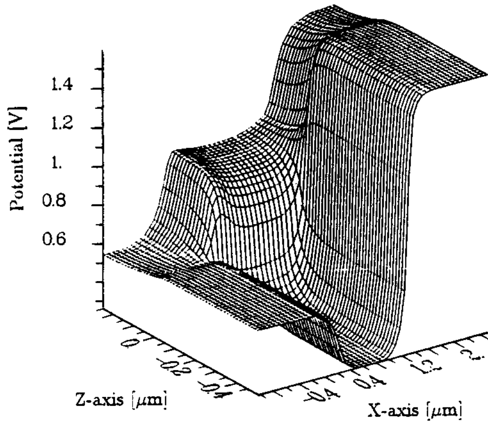

Fig. 8 Detailed view of the surface potential at the channel edge along the channel length at bias U_G = 0.5 V

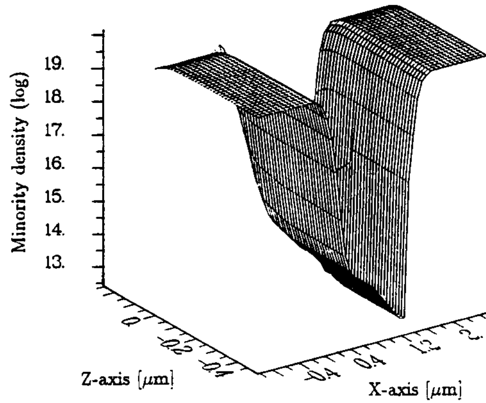

Fig. 9 Detailed view of the minority carrier density at the channel edge along the channel length at bias U_G = 0.5 V

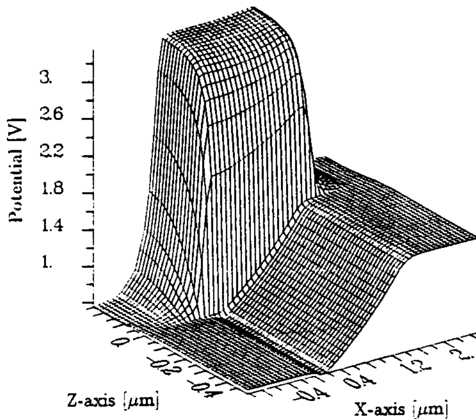

Fig. 10 Detailed view of the surface potential at the channel edge along the channel length at bias U_G = 3.0 V

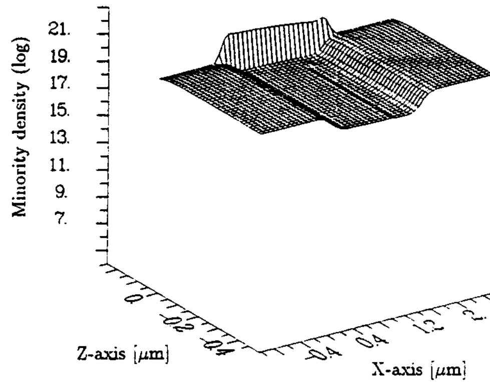

Fig. 11 Detailed view of the minority carrier density at the channel edge along the channel length at bias U_G = 3.0 V

effects depends on the gradient of the "bird's beak" and the channel width. A high gradient in the field-oxide shape results in high parasitic current at the channel edge; this effect is less significant for low gradients. Narrow channel devices with high gradient have much higher currents than predicted by two-dimensional calculations while the agreement with two-dimensional simulations is good for wide channel devices in any case. Using a low gradient in the bird's beak yields a very smooth potential distribution rather than a nearly rectangular shape.

4. Conclusion

The shrinking dimensions of the elements of integrated circuits require suitable process and device models in physics and mathematics for accurate simulation. Although two-dimensional software tools are adequate for many questions the advanced VLSI tech-

nology leads to serious problems which can be investigated rigorously only by fully three-dimensional simulations.

One important drawback of three-dimensional process and device modeling is the enormous amount of computer resources required. The calculations presented in this paper have been carried out on a host computer with 64 MB core memory and one million floating point operations per second. In order to obtain the results of the ion implantation into the trench (section 2.1) about 10^8 particles had to be investigated. The two-dimensional simulation used 0.8 CPU-hours while the three-dimensional one required about 5 CPU-hours. A straightforward Monte Carlo simulation, i.e. without the special acceleration methods implemented in the program package, would have used about 800 CPU-hours. The situation for three-dimensional device modeling is rather similar: the three-dimensional simulation of a MOSFET at difficult bias conditions may require up to 100 CPU-hours. Such a time is only acceptable if just one program run is needed to solve a special problem. However, the calculation of the characteristics, for instance, would not be completed within a reasonable time. Of course nowadays there exist computers which are much faster than the one mentioned above but unfortunately not each investigator has permanent access to such a super-computer. Therefore, three-dimensional process and device modeling actually do not replace the two-dimensional activities, but are absolute necessities for a complete solution.

5. Acknowledgement

This work was considerably supported by the research laboratories of Siemens AG at Munich, F.R.G., the research laboratories of Digital Equipment Corporation at Hudson, U.S.A., and the "Fond zur Förderung der wissenschaftlichen Forschung" under contract S43/10. The authors are indebted to Professor. H. Pötzl for many critical and stimulating discussions.

6. References

[1] Hobler, G. and Selberherr, S., "Efficient two-dimensional Monte Carlo simulation of ion implantation", *Proc. NASECODE V Conf.*, pp. 225–230, 1987.

[2] Budil, M., Pötzl, H., Stingeder, G., Grasserbauer, M. and Goser, K., "A new model of anomalous phosphorus diffusion in silicon", *Proc. of the 15th Internat. Conf. on Defects in Semiconductors,* 1988.

[3] Hobler, G., Langer, E. and Selberherr, S., "Two-dimensional modeling of ion implantation with spatial moments", *Solid State Electron.*, vol. 30, no. 4, pp. 445–455, 1987.

[4] Morehead, F.F. and Hodgson, R.T., "A simple model for the transient, enhanced diffusion of ion-implanted phosphorus in silicon", *Mat. Res. Soc. Symp. Proceedings,* vol. 35, pp. 341–346, 1985.

[5] Jüngling, W., Pichler, P., Selberherr, S., Guerrero, E. and Pötzl, H., "Simulation of critical IC-fabrication processes using advanced physical and numerical methods", *IEEE Trans. on Electron. Devices, Joint Spec. Issue on VLSI,* vol. ED-32, no. 2, pp. 156–167, 1985.

[6] Selberherr, S., "Analysis and simulation of semiconductor devices", Springer, Vienna, 1984.

[7] Gummel, H.K., "A self-consistent iterative scheme for one-dimensional steady state transistor calculations", *IEEE Trans. Electron. Devices,* vol. ED-11, pp. 455–465, 1964.

[8] Hess, K. and Iafrate, G.J., "Theory and applications of near ballistic transport in semiconductors", *Proc. IEEE,* vol. 76, pp. 519–532, 1988.

[9] Robertson, P.J. and Dumin, D.J., "Ballistic transport and properties of submicrometer silicon MOSFETs from 300 to 4.2 K", *IEEE Trans. Electron. Devices,* vol. ED-33, pp. 494–498, 1986.
[10] Baccarani, G., "Physics of submicron devices", *Proc. VLSI Process and Device Modeling,* pp. 1-23, Katholieke Universiteit Leuven, 1983.
[11] Blotekjaer, K., "Transport equations for electrons in two-valley semiconductors", *IEEE Trans. Electron. Devices,* vol. ED-17, pp. 38–47, 1970.
[12] Frey, J., "Transport physics for VLSI", in: *Introduction to the Numerical Analysis of Semiconductor Devices and Integrated Circuits,* pp. 51–57, Boole Press, Dublin 1981.
[13] Selberherr, S., Griebel, W. and Pötzl, H., "Transport physics for modeling semiconductor devices", in: *Simulation of Semiconductor Devices and Processes,* pp. 133–152, Pineridge Press, Swansea, 1984.
[14] Sai-Halasz, G.A., "Processing and characterization of ultra small silicon devices", *Proc. ESSDERC Conf.,* pp. 71–80, 1987.
[15] Shahidi, G.G., Antoniadis, D.A. and Smith, H.I., "Electron velocity overshoot at 300 K and 77 K in silicon MOSFETs with submicron channel length", *Proc. IEDM,* pp. 824–825, 1986.
[16] Ali-Omar, M. and Reggiani, L., "Drift and diffusion of charge carriers in silicon and their empirical relation to the electric field", *Solid State Electron.,* vol. 30, pp. 693-697, 1987.
[17] Canali, C., Majni, G., Minder, R. and Ottaviani, G., "Electron and hole drift velocity measurements in silicon and their empirical relation to electric field and temperature", *IEEE Trans. Electron. Devices,* vol. ED-22, pp. 1045-1047, 1975.
[18] Li, S.S. and Thurber, W.R., "The dopant density and temperature dependence of electron mobility and resistivity in n-type silicon", *Solid State Electron.,* vol. 20, pp. 609–616, 1977.
[19] Caughey, D.M. and Thomas, R.E., "Carrier mobilities in silicon empirically related to doping and field", *Proc. IEEE,* vol. 52, pp. 2192–2193, 1967.
[20] Henning, A.K., Chan, N.N., Watt, J.T. and Plummer, J.D., "Substrate current at cryogenic temperatures: meausrements and a two-dimensional model for CMOS technology", *IEEE Trans. Electron. Devices,* vol. ED-34, pp. 64–74, 1987.
[21] Arora, N.D., Hauser, J.R. and Roulston, D.J., "Electron and hole mobilities in silicon as a function of concentration and temperature", *IEEE Trans. Electron. Devices,* vol. ED-29, pp. 292–295, 1982.
[22] Dorkel, J.M. and Leturcq, Ph., "Carrier mobilities in silicon semi-empirically related to temperature, doping and injection level", *Solid State Electron.,* vol. 24, pp. 821–825, 1981.
[23] Seavey, M., private communication, 1987.
[24] Arora, N.D. and Gildenblat, G.S., "A semi-empirical model of the MOSFET inversion layer mobility for low-temperature operation", *IEEE Trans. Electron. Devices,* vol. ED-34, pp. 89-93, 1987.
[25] Hiroki, A., Odanaka, S., Ohe, K. and Esaki, H., "A mobility for submicrometer MOSFET device simulations", *IEEE Electron. Device Lett.,* vol. EDL-8, pp. 231-233, 1987.
[26] Nishida, T. and Sah, C.T., "A physically based mobility model for MOSFET numerical simulation", *IEEE Trans. Electron. Devices,* vol. ED-34, pp. 310–320, 1987.
[27] Baccarani, G. and Wordeman, M.R., "Transconductance degradation in thin-oxide MOSFETs", *Proc. IEDM,* pp. 278–281, 1982.
[28] Baccarani, G. and Wordeman, M.R., "Transconductance degradation in thin-oxide MOSFETs", *IEEE Trans. Electron. Devices,* vol. ED-30, pp. 1295–1304, 1983.
[29] Faricelli, J., private communication, 1987.

[30] Jaggi, R. and Weibel, H., "High-field electron drift velocities and current densities in silicon", *Helv. Phys. Acta,* vol. 42, pp. 631–632, 1969.
[31] Jaggi, R., "High-field drift velocities in silicon and germanium", *Helv. Phys. Acta,* vol. 42, pp. 941–943, 1969.
[32] Hänsch, W. and Selberherr, S., "MINIMOS 3: a MOSFET simulator that includes energy balance", *IEEE Trans. Electron Devices,* vol. ED-34, pp. 1074–1078, 1987.
[33] Canali, C. and Ottaviani, G., "Saturation values of the electron drift velocity in silicon between 300 K and 4.2 K", *Physics Lett.,* vol. 32A, pp. 147–148, 1970.
[34] Debye, P.P. and Conwell, E.M., "Electrical properties of n-type germanium", *Physical Review,* vol. 93, pp. 693–706, 1954.
[35] Aoki, M., Yano, K., Masuhara, T., Ikeda, S. and Meguro, S., "Optimum crystallographic orientation of submicron CMOS devices", *Proc. IEDM,* pp. 577–580, 1985.
[36] Aoki, M., Yano, K., Masuhara, T., Ikeda, S. and Meguro, S., "Optimum crystallographic orientation of submicrometer CMOS devices operated at low temperatures", *IEEE Trans. Electron. Devices,* vol. ED-34, pp. 52–57, 1987.
[37] Kinugawa, M., Kakumu, M., Usami, T. and Matsunaga, J., "Effects of silicon surface orientation on submicron CMOS devices", *Proc. IEDM,* pp. 581–584, 1985.
[38] Ahmad, N. and Arora, V.K., "Velocity-field profile of n-silicon: a theoretical analysis", *IEEE Trans. Electron. Devices,* vol. ED-33, pp. 1075–1077, 1986.
[39] Baccarani, G. and Wordeman, M.R., "An investigation of steady-state velocity overshoot in silicon", *Solid State Electron.,* vol. 28, pp. 407–416, 1985.
[40] Thurner, M. and Selberherr, S., "The extension of MINIMOS to a 3-D simulation program", *Proc. NASECODE V Conf.,* pp. 327-332, 1987.